Supplement for

Coastal emissions modify the composition and properties of marginal sea aerosols

Kuanyun Hu[1], Narcisse Tsona Tchinda[1], Kun Li[1], Hartmut Herrmann[2,3], Jianlong Li[1,*], Lin Du[1,3,4,*]

[1]Qingdao Key Laboratory for Prevention and Control of Atmospheric Pollution in Coastal Cities, Environment Research Institute, Shandong University, Qingdao 266237, China

[2]Atmospheric Chemistry Department (ACD), Leibniz Institute for Tropospheric Research (TROPOS), Leipzig 04318, Germany

[3]School of Environmental Science and Engineering, Shandong University, Qingdao 266237, China

[4]State Key Laboratory of Microbial Technology, Shandong University, Qingdao 266237, China.

[*]Correspondence to: Lin Du (lindu@sdu.edu.cn); Jianlong Li (jianlongli@sdu.edu.cn)

Text S1: Detailed experimental procedures for the measurement of carbonaceous species and water-soluble ions

Organic carbon and elemental carbon were determined by a semi-continuous OC/EC analyzer (Dual-oven model, Sunset Laboratory Inc., USA). Before measurement, a sucrose standard solution was used to calibrate the instrument. A portion of filter (20 cm^2) of each sample was ultrasonically extracted with 20 mL deionized water for 60 min. Then, extracts were filtered using a 0.22 μm PTFT filter to remove insoluble substances. Then, the extracts were divided into two equal parts. One part was used for WSOC quantitation using a total organic carbon (TOC) analyzer (TOC–5000, Shanghai Metash Instruments Co., Ltd, China). Each sample was measured at least three times until the relative standard deviation was less than 3%.

Another part was further separated into two fractions using a solid-phase extraction (SPE) column (Oasis HLB, 6 cc, 200 mg; Waters). Briefly, the extracts were acidified to pH 2 using HCl, then passed through the SPE column. The fraction not retained in the SPE column was called HPWSOC and the fraction retained in the SPE column was called HULIS. HULIS were further eluted using 3 mL methanol containing 2% ammonia (wt). The eluent was blown to dry under nitrogen flow. The residual was then redissolved in 10 mL water to obtain carbon content in HULIS following the same procedure as WSOC.

For the measurement of water–soluble ions (Na^+, NH_4^+, K^+, Mg^{2+}, Ca^{2+}, Cl^-, NO_3^-,

40 SO_4^{2-}), a portion (10 cm^2) of the filter was ultrasonically extracted with 10 mL deionized
41 water for 60 min. The extracts were thereafter filtered using a 0.22 μm PTFE filter and
42 analyzed using an ion chromatograph (Dionex ICS-600, Thermo Fisher Scientific,
43 USA). The calculation method for non–sea–salt (nss) ions is as follows：

44 $$nss\text{-}X=X\text{-}f\times Na^{+}_{aerosol}$$

45 where $nss-X$ is the concentration (μg m^{-3}) of a nss–ion in aerosols, X is the
46 concentration of a water–soluble ion in aerosols, f is the mass ratio of various ions in
47 seawater to Na^+. Here, f is 0.037 for K^+, 0.12 for Mg^{2+}, 0.0385 for Ca^{2+}, 1.8059 for
48 Cl^- and 0.2516 for SO_4^{2-} (Edwards et al., 2024).

49

50 **Text S2: Calculation of carbon stable isotope ratio and the Bayesian mixing model**

51 Briefly, carbon stable isotope ratio ($\delta^{13}C_{TC}$) is calculated using the following
52 equation (Major et al., 2021):

53 $$\delta^{13}C_{TC}\ (‰) = [(^{13}C_{TC}/^{12}C_{TC})_{sample}/(^{13}C_{TC}/^{12}C_{TC})_{standard}\text{-}1]\times 1000$$

54 where $(^{13}C/^{12}C)_{sample}$ and $(^{13}C_{TC}/^{12}C_{TC})_{standard}$ are the atomic ratio of ^{13}C to ^{12}C in the
55 sample and in the Vienna Pee Dee Belemnite (VPDB) standard, respectively.

56 The Bayesian mixing model was performed using MixSIR package inserted in the R
57 software. The specific principle of Bayesian mixing model can be found in a different
58 study (Zhang et al., 2023). In the analysis process, three files need to be inputted: the
59 measured $\delta^{13}C$ file, the source file, and the isotope fractionation file. According to the

above previous study and the actual environment of the eastern marginal seas of China, we chose four sources: biomass burning (including C3 plant and C4 plant), fossil fuel combustion (coal and Liquid fossil fuel), dust and marine source. The endnumber of each source is shown in Table S7. The isotope fractionation is also considered in this study. All in all, we tested three run modes: short, normal and long. Gelman-Rubin Diagnostic and Geweke Diagnostic were used to verify the rationality of the results. Generally, the Gelman diagnostic should be < 1.05. In the three Markov chains Monte Carlo simulations, we would expect 5% variables to be outside +/-1.96. The diagnostic results are shown in Table S8. Generally, there is no significant difference of source contribution between three run modes.

Text S3 PMF model

The basic principle of PMF model assumes that the origin dataset X is an $i \times j$ matrix. i is the number of samples and j is the number of chemical components. X can be decomposed into two matrices: factor contributions (G) and factor profiles (F):

$$X_{ij} = \sum_{k=1}^{p} G_{ik} F_{kj} + e_{ij}$$

where p is the number of factors, e_{ij} is the residual for each sample/species. The final factor contributions and profiles are derived by the PMF model minimizing the objective function Q:

$$Q=\sum_{i=1}^{n}\sum_{j=1}^{m}\left[\frac{X_{ij}-\sum_{k=1}^{p}G_{ik}F_{kj}}{u_{ij}}\right]^2$$

where u_{ij} is the uncertainty.

There are two Q values (Q (True) and Q (Robust)) and the PMF model seeks a minimal Q. The point where Q (Robust) ≈ Q (True) is considered the optimal solution for the PMF model factorization.

u_{ij} is calculated using the following two equations:

$$u_{ij}=\frac{5}{6}MDL$$

$$u_{ij}=\sqrt{EF\times C^2+0.5\times MDL^2}$$

where MDL is the detection limit of the method, and EF is error fraction which is usually set as 0.1 or 0.2 (Liu et al., 2024). In this study, EF is set as 0.1. C is the species concentration.

The optimal solution, or in other words, the most suitable number of factors are evaluated by Q (True)/Q (Robust), the Displacement Error Estimation and the Bootstrap Error Estimation. Theoretically, Q (True)/Q (Robust) will decrease when the number of factors increases. When the number of factors exceeds a certain value, Q (True)/Q (Robust) changes slowly, which indicates that this number of factors may be suitable. When there are no non-zero values in the row of dQ_{max} = 4 in Displacement Error Estimation while matching rate can reach 80% for all factors in the Bootstrap Error Estimation, this indicates that the number of factors set at this time is appropriate. The evaluation results are presented in Figure S15.

Text S4 The minimum R squared method (MRS)

In this study, MRS calculation was performed using a plugin developed by Wu & Yu (2016) (Wu and Yu, 2016), embedded in Igor Pro. The initial concept of MRS was proposed by Millet et al. (Millet et al., 2005), and aims to explore the inherent independency between pollutants from primary emissions (e.g., EC) and products of secondary formation processes (e.g., SOC) to derive the primary ratios (e.g., $(OC / EC)_{pri}$) (Wu and Yu, 2016). Briefly, this method assumes a series of continuous $(OC / EC)_{pri}$, and SOC is independent of EC. For each $(OC / EC)_{pri}$, SOC is calculated using the following equations:

$$POC=(OC/EC)_{pri}\times EC$$

$$SOC=OC-POC$$

Then, the correlation coefficient between SOC and EC is calculated (R^2 (SOC,EC)), and when R^2 is at its minimum, the corresponding $(OC/EC)_{pri}$ is used as the suitable ratio that best represents the primary source feature. The MRS results are shown in Figure S16.

Text S5 PARAFAC analysis

This model simplifies the EEM dataset into a set of trilinear terms and a set of

residuals (Yu et al., 2020; Stedmon and Bro, 2008). Assuming there are *F* fluorescent components in the sample, the fluorescence intensity of the i^{th} sample at the j^{th} emission wavelength and k^{th} excitation wavelength is decomposed into three parts: component score (a), emission loading (b), and excitation loading (c), as follows:

$$X_{ijk}=\sum_{f=1}^{F} a_{if}b_{jf}c_{kf}+\varepsilon_{ijk}$$

where ε_{ijk} is the residual term, a, b and c represent the relative concentration, the emission and the excitation spectra of the component, respectively. The model evaluation results are shown in Figure S17. Split Half analysis shows that 3 fluorescent components are suitable for water–soluble organic matter, and 2 fluorescent components are suitable for non–water soluble organic matter.

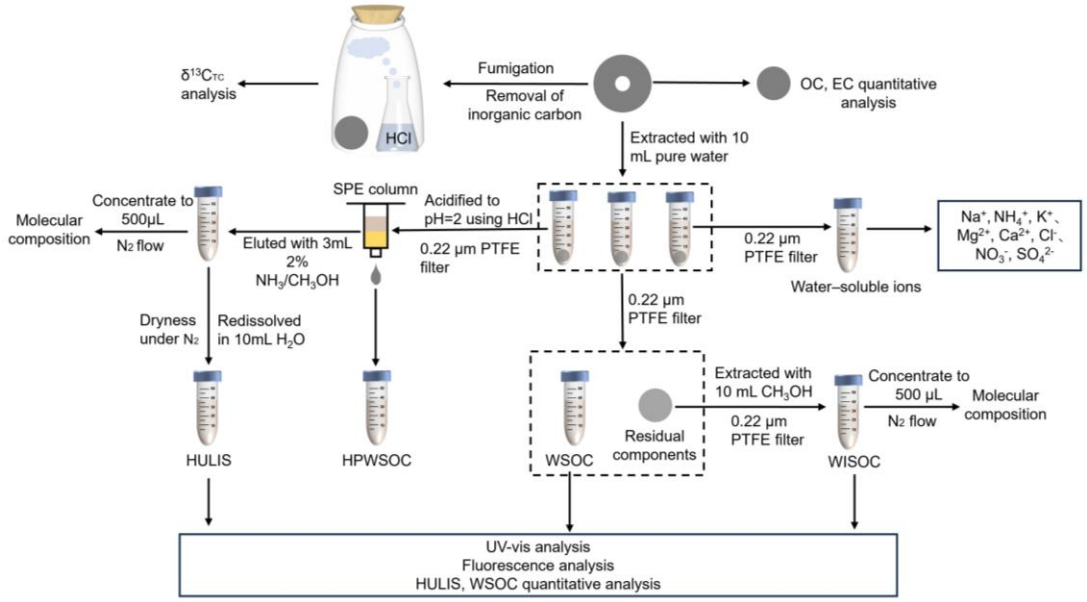

129

130 Figure S1. Basic experimental flowchart.

131

132

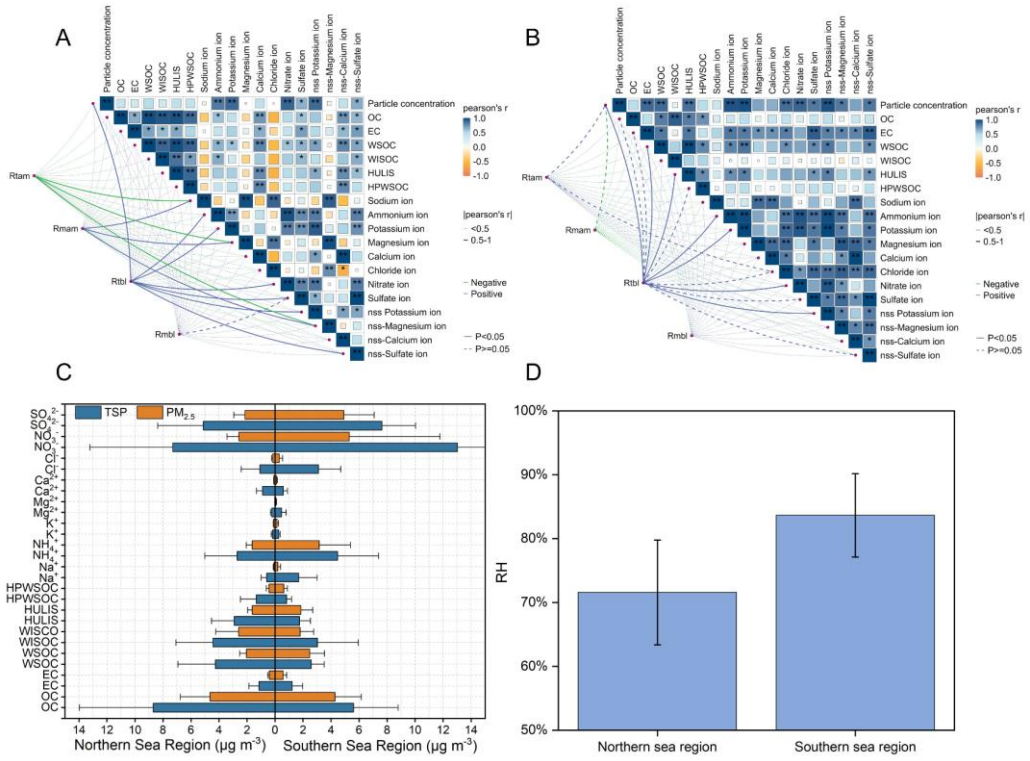

133

134 Figure S2. Correlation map of major components in (A) TSP and (B) $PM_{2.5}$. (C) Concentration

comparison of chemical composition in different sea regions. (D) Comparison of average relative humidity (RH) between northern and southern sea regions.

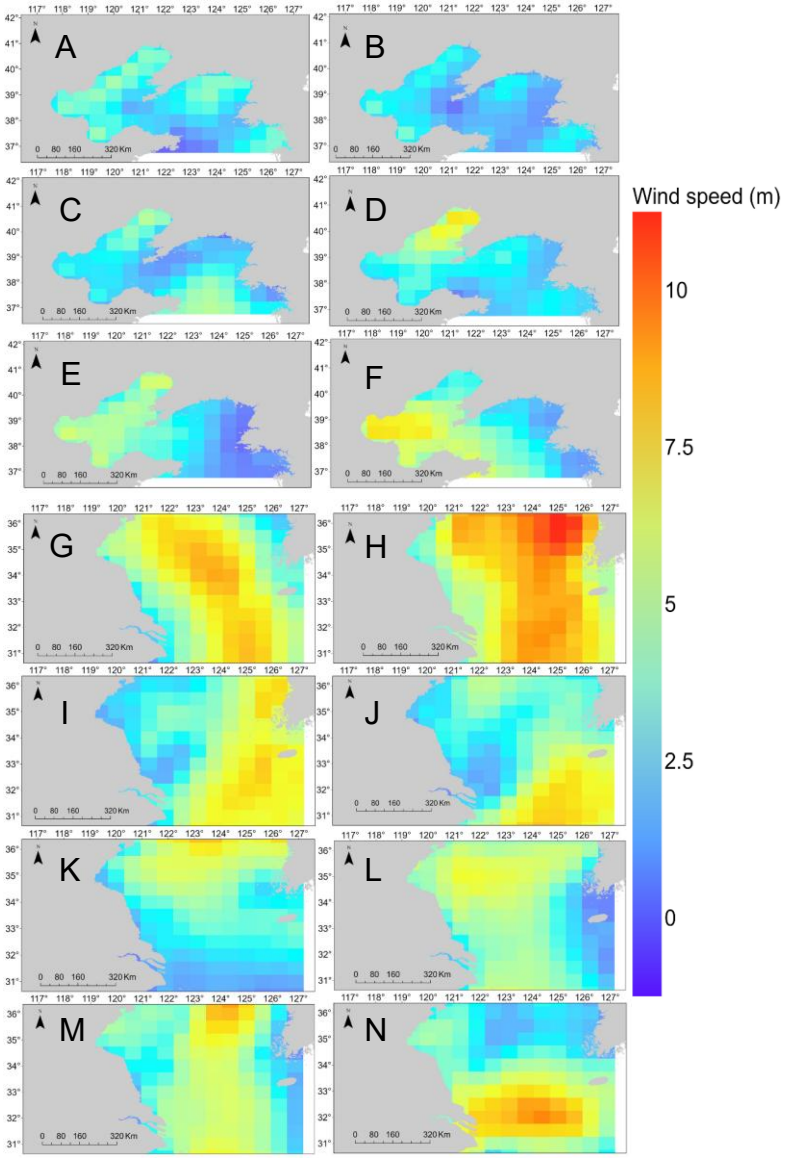

Figure S3. Average daily wind speed at 10m above the sea surface in the northern sea region (A–F) and southern sea region (G–N), during the sampling period.

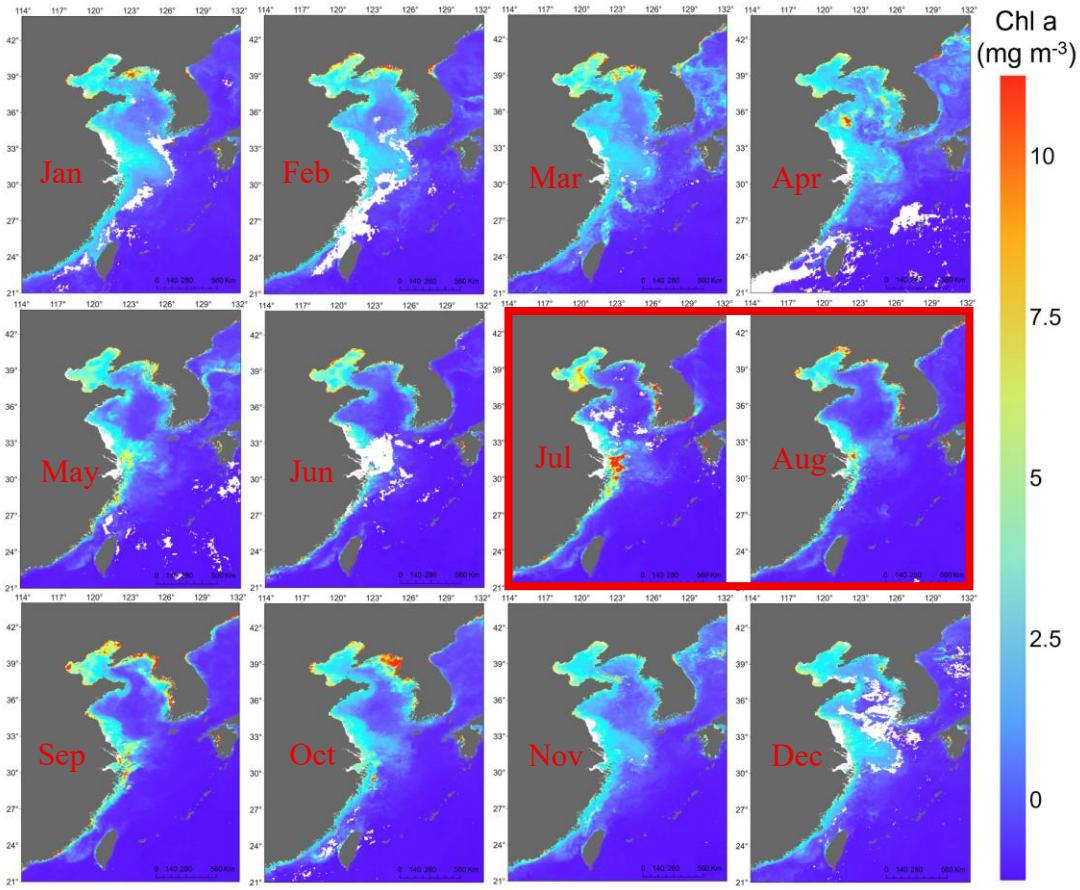

142

143 Figure S4. Changes in sea surface chlorophyll-a concentration in different months of 2023.

144

145

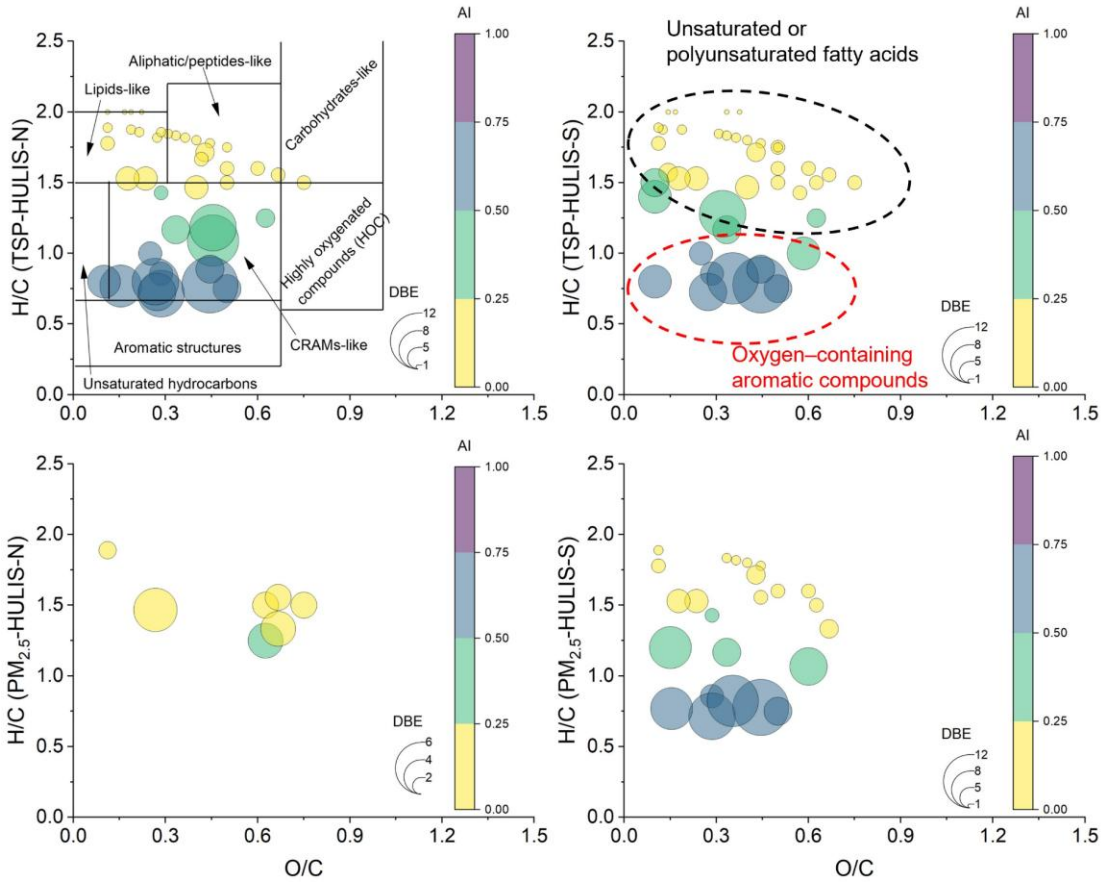

146

147 Figure S5. Major CHO compounds in HULIS.

148

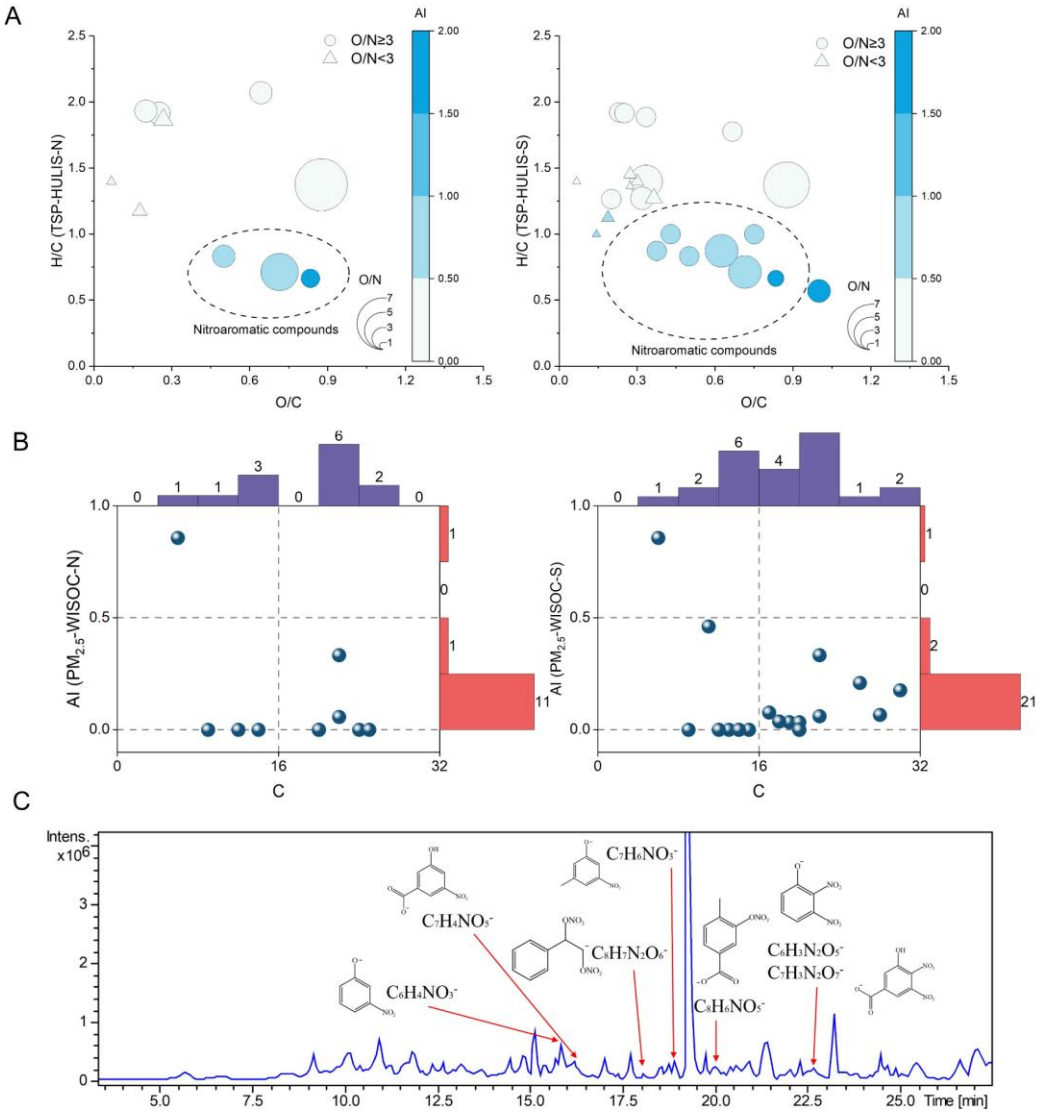

149

150 Figure S6. Major CHON species compounds in (A) HULIS and (B) WISOC. (C) Chromatograms and

151 possible structural formulas of typical nitroaromatic compounds in typical samples. Since CHON

152 compounds in TSP mainly exist in HULIS, while CHON compounds in $PM_{2.5}$ mainly exist in WISOC,

153 feature data are selected here for display.

154

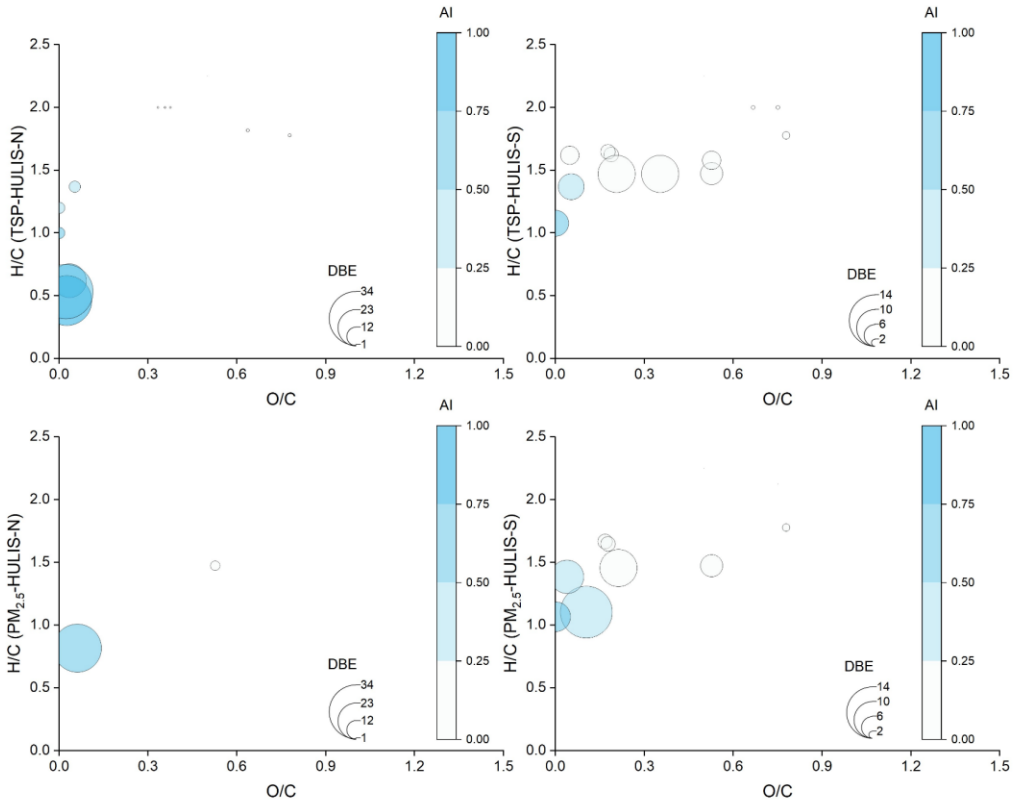

155

156 Figure S7. Typical CHOS compounds in chromatographic peaks with signal-to-noise ratio ≥ 5 in HULIS.

157

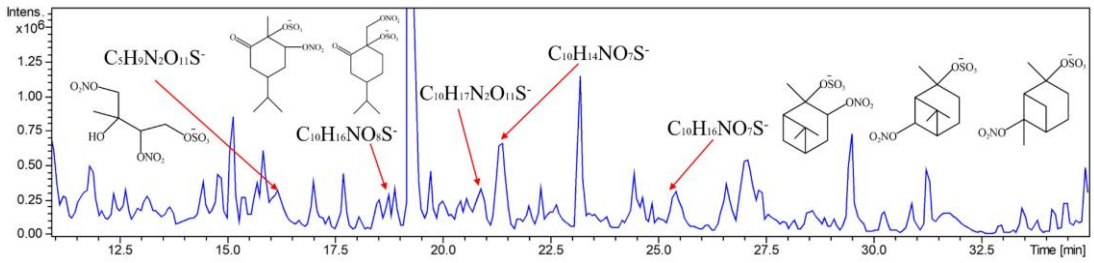

158

159 Figure S8. Chromatograms and possible structural formulas of typical Isoprene and monoterpene

160 derivatives.

161

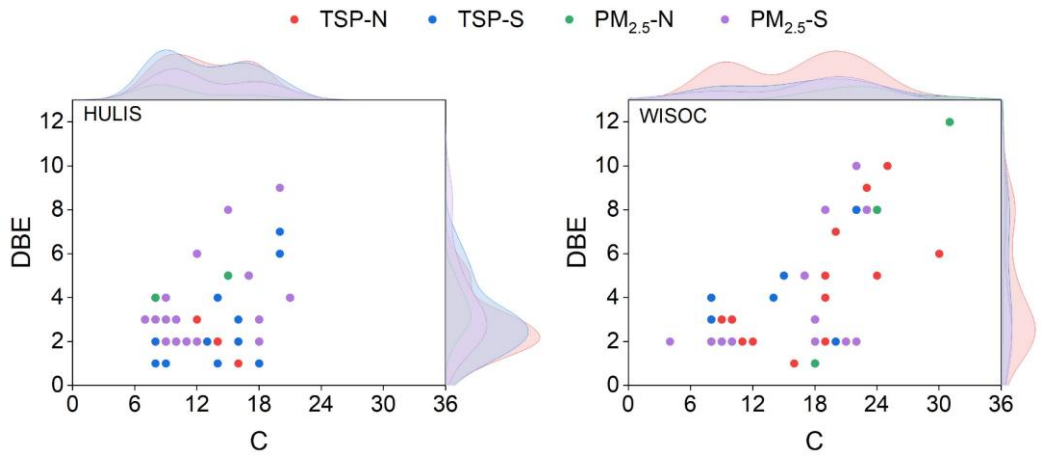

Figure S9. Carbon number and DBE distribution of unsaturated oxygen–containing aliphatic compounds in HULIS and WISOC.

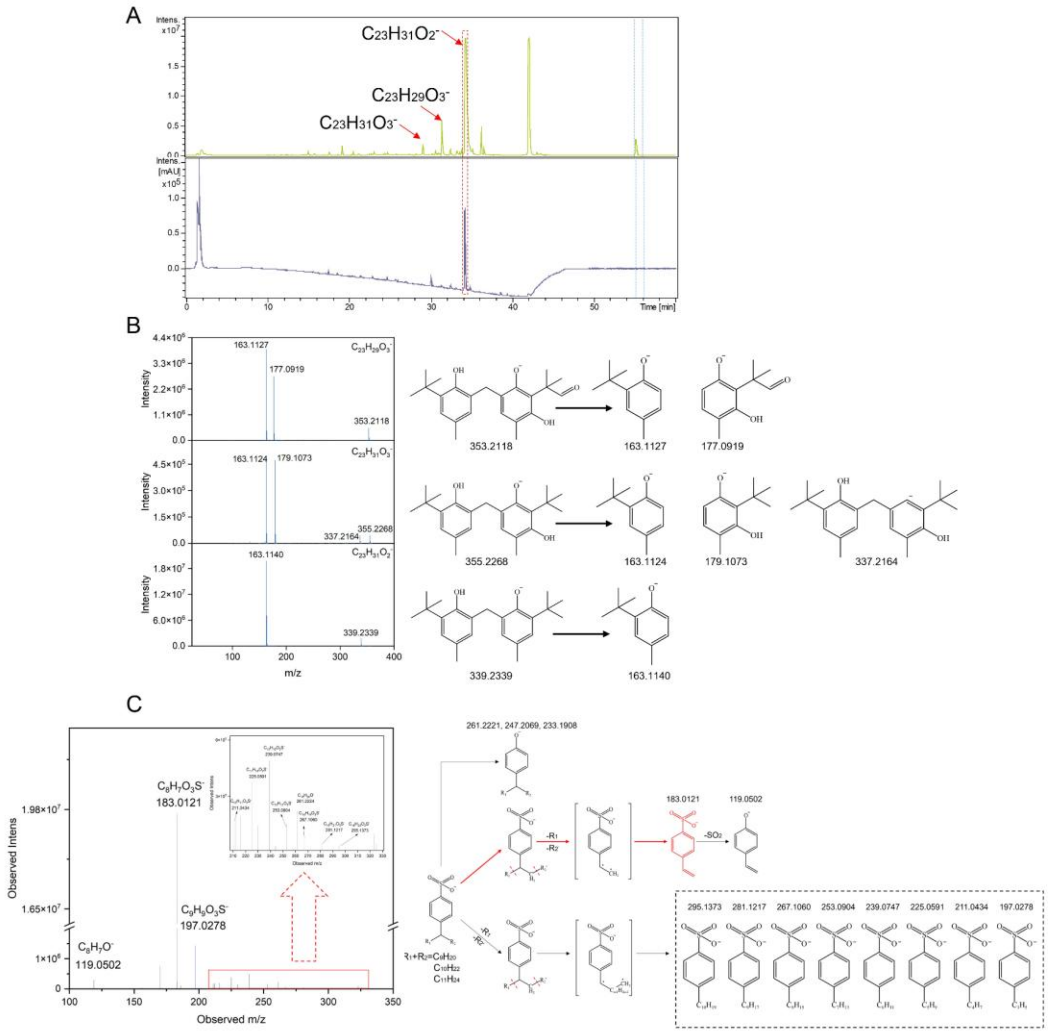

167

168 Figure S10. (A) Chromatographic peaks and light absorption chromatogram of $C_{23}H_{31}O_2^-$ and its

169 derivatives. (B) Secondary mass spectra of $C_{23}H_{31}O_2^-$ and its derivatives and their possible structures. (C)

170 Secondary mass spectra of branched alkylbenzene sulfonate.

171

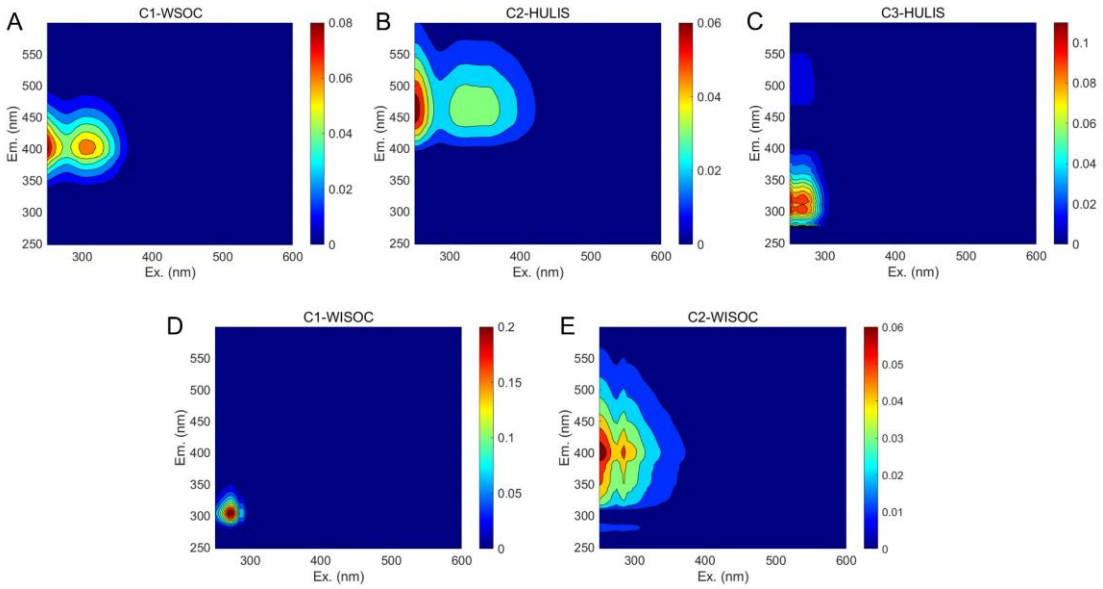

Figure S11. (A) to (C) Fluorescent components in WSOC. C1-WSOC and C2-WSOC are two HULIS components, and C3-WSOC is PRLIS component. (D) Non-nitrogen-containing component and (E) HULIS component in WISOC.

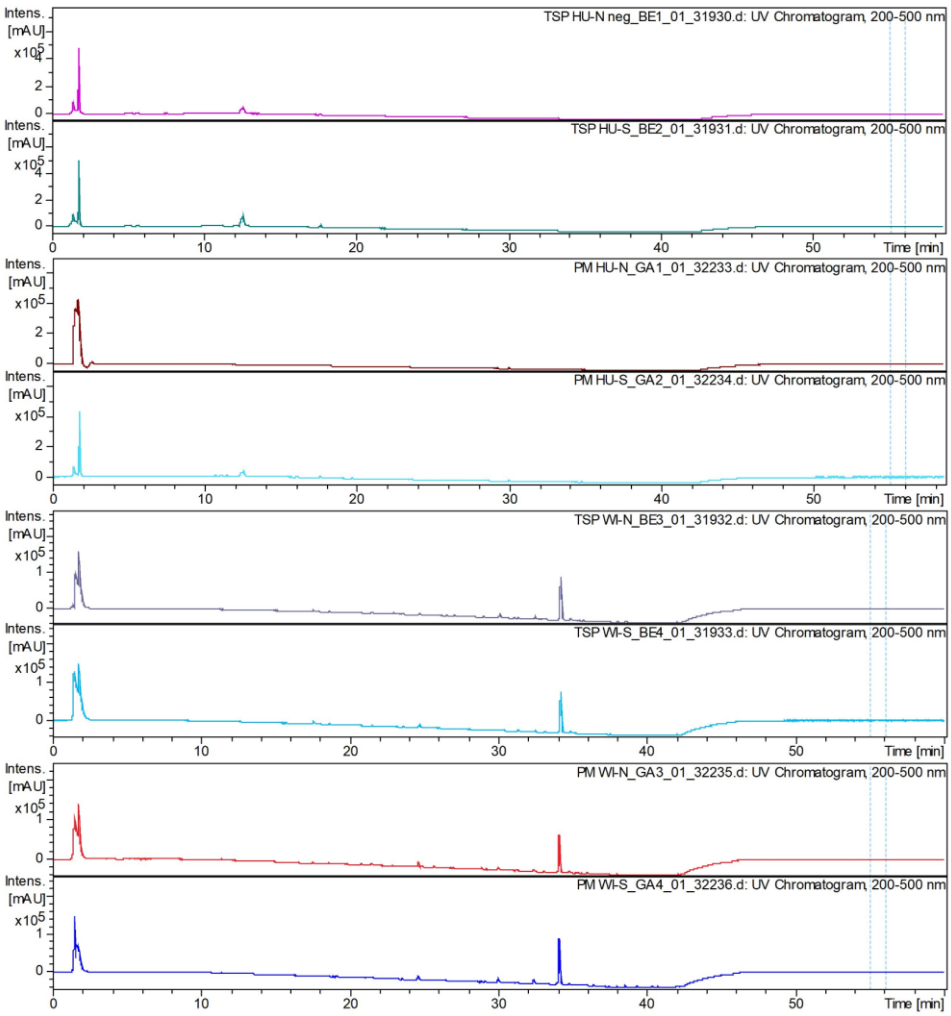

177

178 Figure S12. Absorption spectrum of HULIS and WISOC in the TSP and $PM_{2.5}$ samples.

179

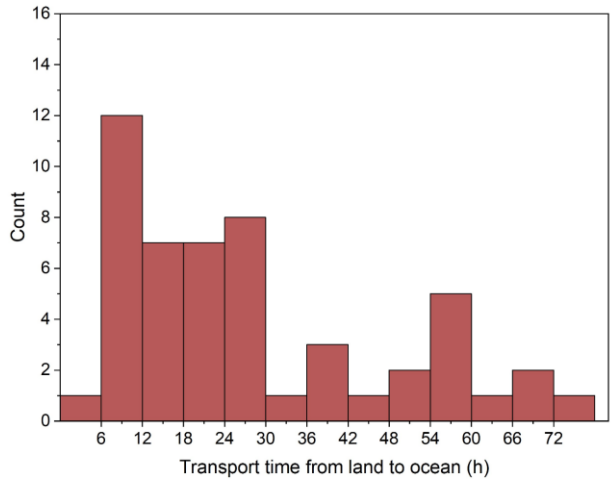

180

181 Figure S13. Transport time for air masses from land to ocean sampling points.

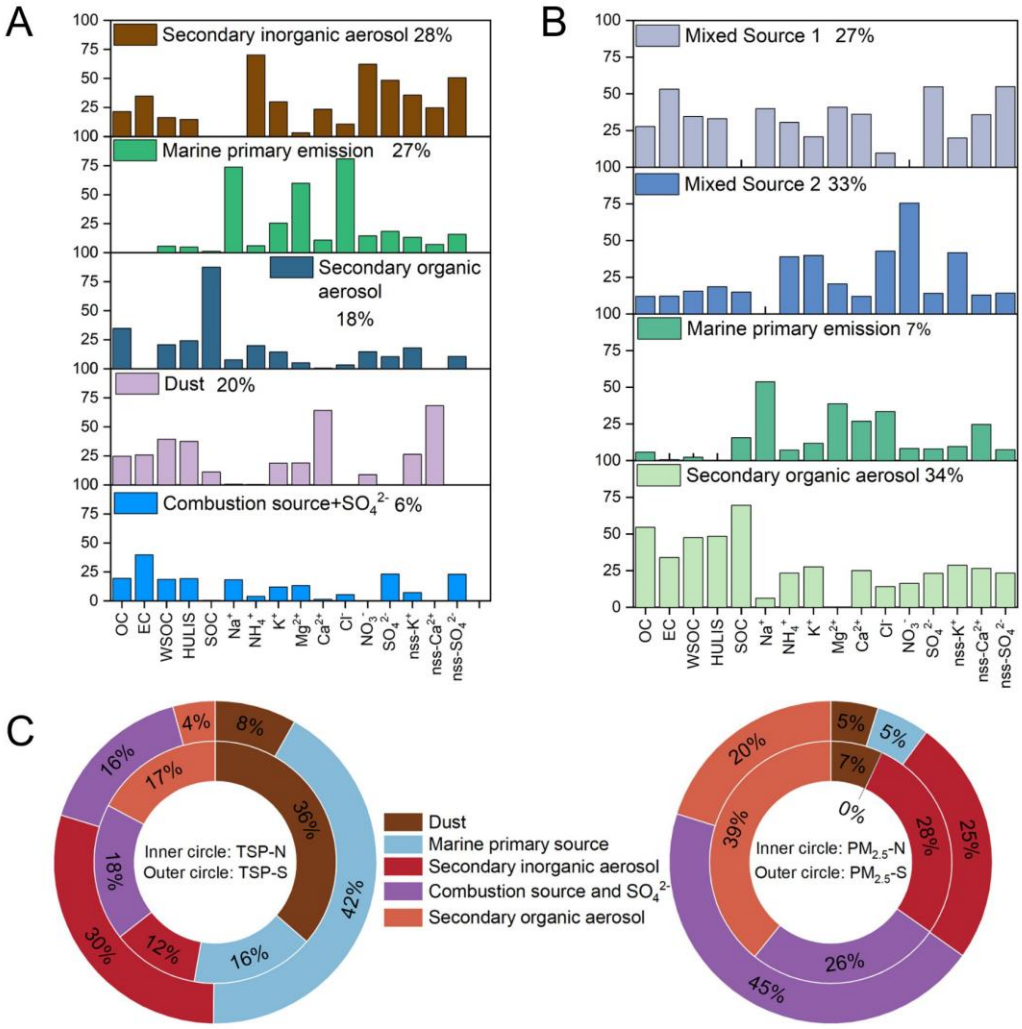

Figure S14. PMF results derived from (A) $PM_{2.5}$ and (B) TSP dataset. (C) Difference of source contribution in sea region contributions derived from PMF model.

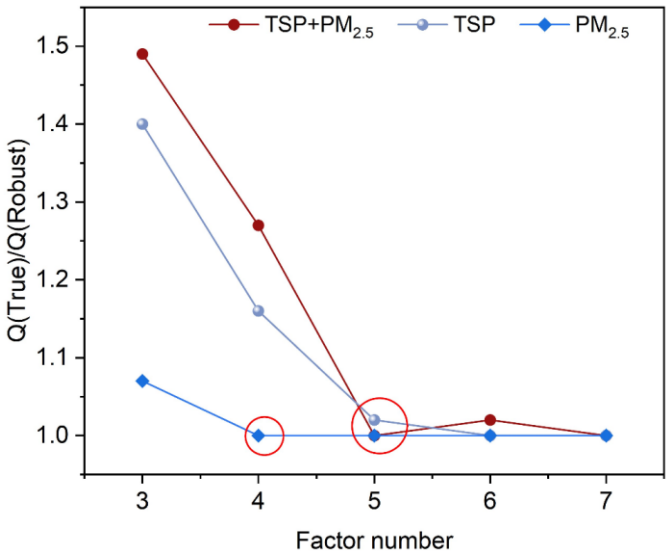

Figure S15. Variation of Q (True)/Q (Robust) with the increase of factor number. The red circles represent the optimal factor number.

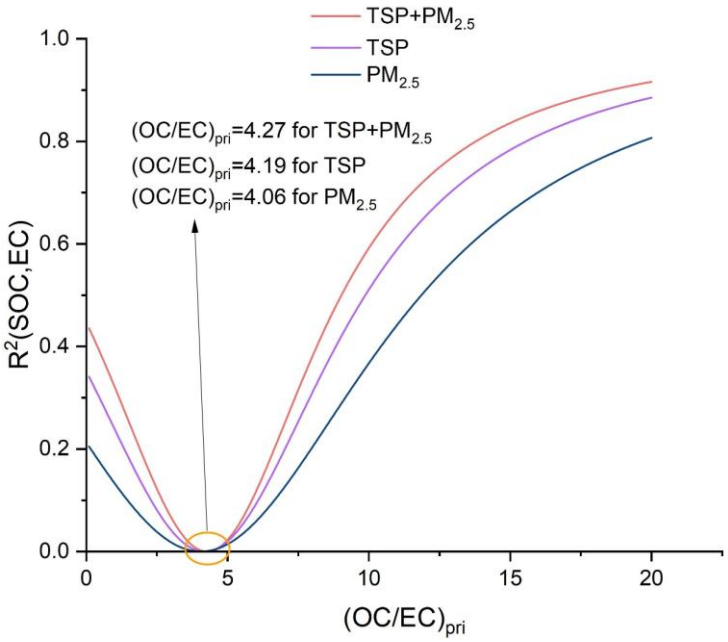

Figure S16. Most suitable $(OC/EC)_{pri}$ corresponding to the minimum R^2.

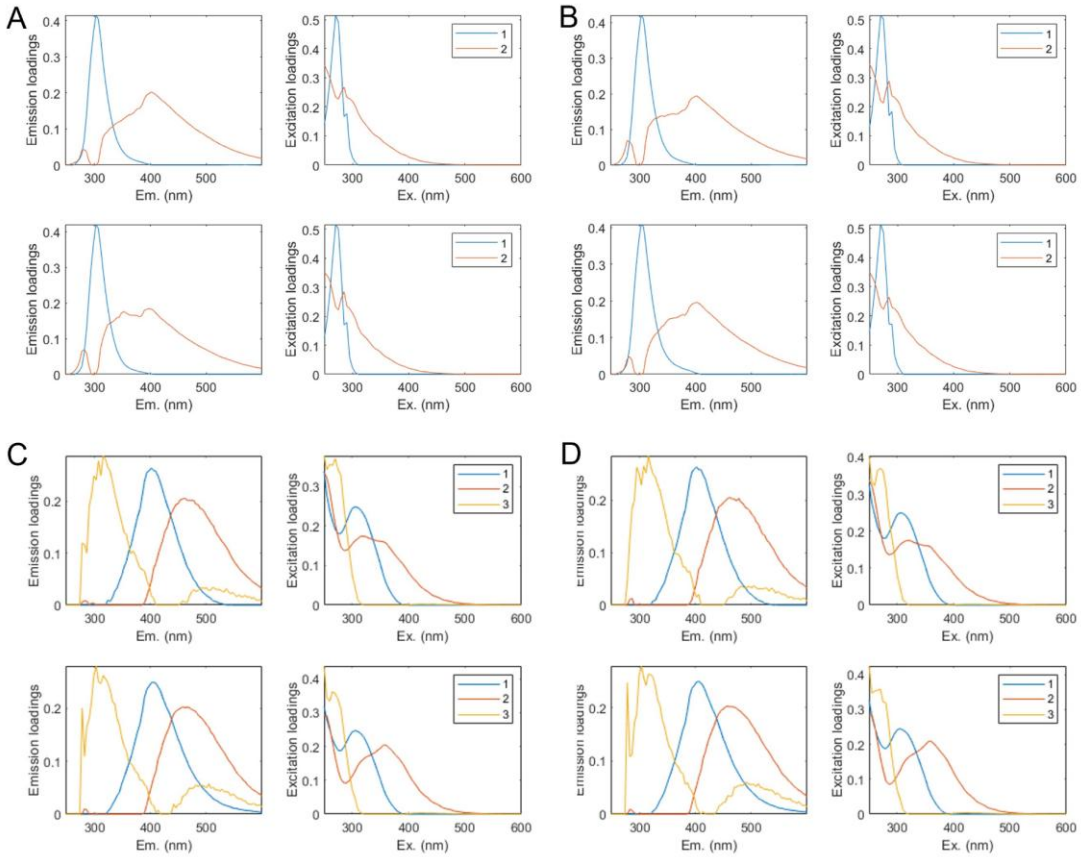

Figure S17. (A) and (B) Split Half analysis of WISOC fluorescent components. (C) and (D) Split Half analysis of WSOC fluorescent components.

Table S1. Comparative summary of carbon component ratios in aerosols from different seasons and regions.

	Region	WSOC/OC	OC/EC	Season	Particle	Reference
Marginal sea	Bohai and Northern Yellow Sea	0.49 ± 0.03	7.32 ± 2.19	Summer	TSP	This study
	Southern Yellow Sea	0.56 ± 0.19	5.58 ± 2.27	Summer		
	Bohai and Northern Yellow Sea	0.48 ± 0.09	12.11 ± 75.22	Summer	$PM_{2.5}$	
	southern Yellow Sea	0.58 ± 0.08	5.59 ± 2.68	Summer		
Inland city	Beijing	0.555	2.5 ± 0.4	Summer	PM_{10}	(Tang et al., 2016)
	Beijing	0.565	4.1 ± 1.6	Spring		
	Beijing	0.516	2.7 ± 0.7	Autumn		
	Beijing	0.462	3.3 ± 0.7	Winter		
	Himalaya	0.57 ± 0.10	5.67 ± 1.24	Winter	–	(Ramya et al., 2023)
	Himalaya	0.63 ± 0.03	5.23 ± 2.5	Monsoon		
	IGP-biomass burning night	0.5 ± 0.1	11.3 ± 4.6	Winter	$PM_{2.5}$	(Srinivas et al., 2016)
	Beijing	0.55 ± 0.1	2.2 ± 1.3	Summer	$PM_{2.5}$	(Pathak et al., 2011)
	Lanzhou	0.4±0.1	2.5±0.8	Summer		
Marginal sea	Northwest Indian Ocean	0.72 ± 0.15	3.3 ± 1.62	Winter	–	(Ramya et al., 2023)
	Bohai and Yellow Sea	0.68 ± 0.12	5.03 ± 1.45	Summer	TSP	(Zhao et al., 2023)
	Bohai and Yellow Sea	0.35 ± 0.08	15.47 ± 4.91	Winter		
	Bohai Sea	0.66 ± 0.13	4.34 ± 3.05	Summer	TSP	

	Yellow Sea	0.71 ± 0.13	5.63 ± 1.99	Summer		(Ding et al., 2019)
	Northern Indian Ocean	0.45 ± 0.12	6.7 ± 1.7	Winter	$PM_{2.5}$	(Srinivas and Sarin, 2013)
	Northern Indian Ocean	0.77 ± 0.15	1.67 ± 0.38	Winter		(Panda et al., 2023)
	Eastern Indian Ocean	0.15 ± 0.03	1.9 ± 0.68	Winter		
	Bay of Bengal	0.53 ± 0.04	4.6 ± 1.2	Winter		(Nayak et al., 2022)
Coastal city	Coastal site-Huaniao island	0.66 ± 0.18	6.67 ± 3.40	Winter	$PM_{2.5}$	(Li et al., 2022)
	Coastal site-Dongying		13.08 ± 3.55	Summer	$PM_{2.5}$	(Zhang et al., 2022)
	Tianjin	0.6 ± 0.12	7.99 ± 2.08	Winter	$PM_{2.5}$	(Chen et al., 2023)
	Qingdao	0.55 ± 0.12	6.45 ± 1.15	Winter		
	Shanghai	0.61 ± 0.07	10.05 ± 2.69	Winter		
	Shanghai	0.35 ± 0.1	1.7 ± 0.6	Summer	$PM_{2.5}$	(Pathak et al., 2011)
	Guangzhou	0.32 ± 0.1	1.6 ± 0.7	Summer		
Open ocean	Northwest Pacific Ocean	0.56 ± 0.19	4.11 ± 1.19	Spring	TSP	(Boreddy et al., 2018)
		0.44 ± 0.17	19 ± 16.7	Summer		
		0.45 ± 0.19	12.2 ± 9.07	Autumn		
		0.69 ± 0.14	4.85 ± 2.01	Winter		

Table S2. Proportion of sea salt and non-sea salt ions calculated based on different Na^+ proportion from the ocean.

Proportion of Na^+ from ocean		Sea salt proportion	Non-Sea salt proportion
100 % Na^+	TSP	0.16±0.14	0.84±0.14
	$PM_{2.5}$	0.04±0.03	0.96±0.03
50 % Na^+	TSP	0.07±0.06	0.93±0.06
	$PM_{2.5}$	0.02±0.02	0.98±0.02
20 % Na^+	TSP	0.04±0.03	0.96±0.03
	$PM_{2.5}$	0.01±0.01	0.99±0.01

Table S3. Molecular characteristics of two main types of organic components.

O/C_w	H/C_w	N/C_w	S/C_w	O/N_w	O/S_w	DBE_w	AI_w	OSc_w	Number
TSP-HULIS-N									
0.40	1.27	0.04	0.03	1.27	2.69	8.89	0.35	-0.47	1913
TSP-HULIS-S									
0.41	1.37	0.04	0.03	1.58	2.65	7.30	0.33	-0.55	1401
TSP-WISOC-N									
0.27	1.54	0.01	0.03	0.38	2.02	5.62	0.21	-1.01	715
TSP-WISOC-S									
0.21	1.56	0.01	0.03	0.33	1.88	5.46	0.19	-1.15	323
$PM_{2.5}$-HULIS-N									
0.33	1.38	0.04	0.02	1.60	2.74	9.06	0.46	-0.72	1663
$PM_{2.5}$-HULIS-S									
0.35	1.34	0.03	0.03	1.11	2.70	8.96	0.31	-0.65	1117
$PM_{2.5}$-WISOC-N									
0.18	1.40	0.02	0.02	0.50	1.28	7.93	0.30	-1.05	489
$PM_{2.5}$-WISOC-S									
0.18	1.42	0.02	0.01	0.46	0.64	7.49	0.27	-1.05	227

N and S denote the northern and southern sea regions, respectively.

Table S4. Major light absorption parameters of TSP and $PM_{2.5}$ in two sea regions.

	TSP			$PM_{2.5}$		
	Abs_{365} (Mm^{-1})	MAE_{365} ($m^2\ g^{-1}$)	AAE	Abs_{365} (Mm^{-1})	MAE_{365} ($m^2\ g^{-1}$)	AAE
WSOC North	1.20 ± 0.68	0.26 ± 0.05	6.68 ± 0.52	0.54 ± 0.13	0.22 ± 0.02	7.01 ± 0.08
WSOC South	1.01 ± 0.42	0.25 ± 0.08	6.98 ± 0.69	0.75 ± 0.49	0.22 ± 0.09	6.74 ± 0.31
HULIS North	0.79 ± 0.46	0.27 ± 0.03	7.56 ± 0.73	0.46 ± 0.12	0.28 ± 0.02	7.40 ± 0.17
HULIS South	0.54 ± 0.30	0.29 ± 0.05	7.55 ± 0.77	0.51 ± 0.32	0.24 ± 0.09	7.41 ± 0.35
WISOC North	0.73 ± 0.38	0.13 ± 0.03	6.34 ± 0.79	0.29 ± 0.12	0.12 ± 0.07	5.56 ± 0.62
WISOC South	0.52 ± 0.18	0.20 ± 0.09	6.16 ± 0.76	0.30 ± 0.15	0.13 ± 0.03	5.97 ± 1.26

Table S5. Molecular characteristics of potential light-absorbing molecules.

	O/C_w	H/C_w	N/C_w	S/C_w	O/N_w	O/S_w	DBE_w	AI_w	OSc_w
TSP-HULIS-N	0.25	1.01	0.01	0.05	0.38	1.74	8.94	0.48	-0.51
TSP-HULIS-S	0.33	1.01	0.03	0.05	0.42	2.15	8.95	0.59	-0.35
TSP-WISOC-N	0.64	1.02	0.03	0.02	0.26	0.73	6.72	0.46	0.26
TSP-WISOC-S	0.71	1.10	0.01	0.01	0.12	0.73	5.11	0.35	0.31
$PM_{2.5}$-HULIS-N	0.16	0.70	0.06	0.02	1.63	2.31	20.32	0.69	-0.39
$PM_{2.5}$-HULIS-S	0.38	0.99	0.02	0.03	0.66	1.58	10.56	0.49	-0.24
$PM_{2.5}$-WISOC-N	0.49	0.92	0.01	0.04	0.09	1.38	7.88	0.50	0.06
$PM_{2.5}$-WISOC-S	1.01	0.88	0.06	0.10	0.72	5.24	6.29	1.30	1.13

N and S indicate the northern and southern sea regions, respectively.

Table S6. MAE_{365} of WSOC in typical urban aerosols in coastal regions.

City	Species	MAE_{365}	Note	Reference
Qingdao	WSOC	0.54 ± 0.37	Day	(Zhan et al., 2022)
		0.51 ± 0.22	Night	
Nanjing	WSOC	0.67 ± 0.20		(Xie et al., 2020)
Shanghai	WSOC	0.55 ± 0.20	Pudong	(Zhou et al., 2022)
		0.51 ± 0.13	Qingpu	
Tianjin	WSOC	0.84 ± 0.22		(Deng et al., 2022)
Shanghai	WSOC	0.55		(Mo et al., 2021)
Guangzhou	WSOC	0.68		

Table S7. Total carbon isotopes and isotope fractionation information of each source input in the Bayesian mixture model.

	Source information		Isotope fractionation	
Source	Mean $\delta 13C_{TC}$	SD $\delta 13C_{TC}$	Mean $\delta 13C_{TC}$	SD $\delta 13C_{TC}$
C3 Plant	-26.1	0.5	0	0.5
C4 Plant	-12.8	0.6	-3.85	3.35
Coal	-23.4	1.3	-0.3	0.9
Liquid fossil fuel	-25.5	1.3	4.2	3.7
Dust	-10.5	4	0	0
Marine emission	-21	1.9	-2.6	0.9

Table S8. Diagnostic results of three run modes in Bayesian mixing model.

Diagnostic results-TSP-isotope fractionation					
Short		Normal		Long	
Gelman Rubin Diagnostic	Geweke Diagnostic	Gelman Rubin Diagnostic	Geweke Diagnostic	Gelman Rubin Diagnostic	Geweke Diagnostic
0>1.01	1	0>1.01	0	1>1.01	4
0>1.05	0	0>1.05	0	0>1.05	0
0>1.1	3	0>1.1	0	0>1.1	0
Diagnostic results-TSP-Non isotope fractionation					
Short		Normal		Long	
Gelman Rubin Diagnostic	Geweke Diagnostic	Gelman Rubin Diagnostic	Geweke Diagnostic	Gelman Rubin Diagnostic	Geweke Diagnostic
0>1.01	0	0>1.01	0	0>1.01	4
0>1.05	0	0>1.05	1	0>1.05	0
0>1.1	0	0>1.1	0	0>1.1	3
Diagnostic results-$PM_{2.5}$-isotope fractionation					
Short		Normal		Long	
Gelman Rubin Diagnostic	Geweke Diagnostic	Gelman Rubin Diagnostic	Geweke Diagnostic	Gelman Rubin Diagnostic	Geweke Diagnostic
1>1.01	0	0>1.01	0	0	3
0>1.05	0	0>1.05	4	0	1
0>1.1	2	0>1.1	2	0	0
Diagnostic results-$PM_{2.5}$-Non isotope fractionation					
Short		Normal		Long	
Gelman Rubin Diagnostic	Geweke Diagnostic	Gelman Rubin Diagnostic	Geweke Diagnostic	Gelman Rubin Diagnostic	Geweke Diagnostic
0>1.01	2	0>1.01	1	0>1.01	3
0>1.05	0	0>1.05	2	0>1.05	0
0>1.1	0	0>1.1	2	0>1.1	0
Diagnostic results-combine TSP and $PM_{2.5}$-isotope fractionation					
Short		Normal		Long	
Gelman Rubin Diagnostic	Geweke Diagnostic	Gelman Rubin Diagnostic	Geweke Diagnostic	Gelman Rubin Diagnostic	Geweke Diagnostic
0>1.01	0	1>1.01	9	1>1.01	0
0>1.05	2	0>1.05	0	0>1.05	0
0>1.1	0	0>1.1	1	0>1.1	1

Diagnostic results-combine TSP and $PM_{2.5}$-Non isotope fractionation					
Short		Normal		Long	
Gelman Rubin Diagnostic	Geweke Diagnostic	Gelman Rubin Diagnostic	Geweke Diagnostic	Gelman Rubin Diagnostic	Geweke Diagnostic
0>1.01	0	0>1.01	0	1>1.01	0
0>1.05	1	0>1.05	2	0>1.05	2
0>1.1	0	0>1.1	3	0>1.1	5

Gelman Rubin Diagnostic column indicates the number of variables greater than these three values. Geweke Diagnostic column indicates the number of variables outside +/-1.96 in three chains.

References

Boreddy, S. K. R., Haque, M. M., and Kawamura, K.: Long-term (2001–2012) trends of carbonaceous aerosols from a remote island in the western North Pacific: an outflow region of Asian pollutants, Atmos. Chem. Phys., 18, 1291-1306, 10.5194/acp-18-1291-2018, 2018.

Chen, H., Yan, C., Fu, Q., Wang, X., Tang, J., Jiang, B., Sun, H., Luan, T., Yang, Q., Zhao, Q., Li, J., Zhang, G., Zheng, M., Zhou, X., Chen, B., Du, L., Zhou, R., Zhou, T., and Xue, L.: Optical properties and molecular composition of wintertime atmospheric water-soluble organic carbon in different coastal cities of eastern China, Sci. Total Environ., 892, 164702, 10.1016/j.scitotenv.2023.164702, 2023.

Deng, J., Ma, H., Wang, X., Zhong, S., Zhang, Z., Zhu, J., Fan, Y., Hu, W., Wu, L., Li, X., Ren, L., Pavuluri, C. M., Pan, X., Sun, Y., Wang, Z., Kawamura, K., and Fu, P.: Measurement report: Optical properties and sources of water-soluble brown carbon in Tianjin, North China – insights from organic molecular compositions, Atmos. Chem. Phys., 22, 6449-6470, 10.5194/acp-22-6449-2022, 2022.

Ding, X., Qi, J., and Meng, X.: Characteristics and sources of organic carbon in coastal and marine atmospheric particulates over East China, Atmos. Res., 228, 281-291, 10.1016/j.atmosres.2019.06.015, 2019.

Edwards, E.-L., Choi, Y., Crosbie, E. C., DiGangi, J. P., Diskin, G. S., Robinson, C. E., Shook, M. A., Winstead, E. L., Ziemba, L. D., and Sorooshian, A.: Sea salt reactivity over the northwest Atlantic: an in-depth look using the airborne ACTIVATE dataset, Atmos. Chem. Phys., 24, 3349-3378, 10.5194/acp-24-3349-2024, 2024.

Li, H., Qin, X., Wang, G., Xu, J., Wang, L., Lu, D., Liu, C., Zheng, H., Liu, J., Huang, K., and Deng, C.: Conjoint impacts of continental outflows and marine sources on brown carbon in the East China sea: Abundances, optical properties, and formation processes, Atmos. Environ., 273, 118959, 10.1016/j.atmosenv.2022.118959, 2022.

Liu, Z., Wang, L., Yan, M., Ben, M., and Cao, R.: Source apportionment of soil heavy metals based on multivariate statistical analysis and the PMF model: A case study

of the Nanyang Basin, China, Environmental Technology & Innovation, 33, 103537, 10.1016/j.eti.2024.103537, 2024.

Major, I., Furu, E., Varga, T., Horváth, A., Futó, I., Gyökös, B., Somodi, G., Lisztes-Szabó, Z., Jull, A. J. T., Kertész, Z., and Molnár, M.: Source identification of PM2.5 carbonaceous aerosol using combined carbon fraction, radiocarbon and stable carbon isotope analyses in Debrecen, Hungary, Sci. Total Environ., 782, 146520, 10.1016/j.scitotenv.2021.146520, 2021.

Millet, D. B., Donahue, N. M., Pandis, S. N., Polidori, A., Stanier, C. O., Turpin, B. J., and Goldstein, A. H.: Atmospheric volatile organic compound measurements during the Pittsburgh Air Quality Study: Results, interpretation, and quantification of primary and secondary contributions, J. Geophys. Res.-Atmos., 110, 10.1029/2004jd004601, 2005.

Mo, Y., Li, J., Cheng, Z., Zhong, G., Zhu, S., Tian, C., Chen, Y., and Zhang, G.: Dual Carbon Isotope‐Based Source Apportionment and Light Absorption Properties of Water‐Soluble Organic Carbon in PM2.5 Over China, J. Geophys. Res.-Atmos., 126, e2020JD033920, 10.1029/2020jd033920, 2021.

Nayak, G., Kumar, A., Bikkina, S., Tiwari, S., Sheteye, S. S., and Sudheer, A. K.: Carbonaceous aerosols and their light absorption properties over the Bay of Bengal during continental outflow, Environ Sci Process Impacts, 24, 72-88, 10.1039/d1em00347j, 2022.

Panda, S., Babu, S. S., Sharma, S. K., Mandal, T. K., Das, T., and Ramasamy, B.: Role of South Asian outflow on the oxidative potential of marine aerosols over the Indian Ocean, Sci. Total Environ., 887, 164105, 10.1016/j.scitotenv.2023.164105, 2023.

Pathak, R. K., Wang, T., Ho, K. F., and Lee, S. C.: Characteristics of summertime PM2.5 organic and elemental carbon in four major Chinese cities: Implications of high acidity for water-soluble organic carbon (WSOC), Atmos. Environ., 45, 318-325, 10.1016/j.atmosenv.2010.10.021, 2011.

Ramya, C. B., Aswini, A. R., Hegde, P., Boreddy, S. K. R., and Babu, S. S.: Water-soluble organic aerosols over South Asia - Seasonal changes and source

characteristics, Sci. Total Environ., 900, 165644, 10.1016/j.scitotenv.2023.165644, 2023.

Srinivas, B. and Sarin, M. M.: Light absorbing organic aerosols (brown carbon) over the tropical Indian Ocean: impact of biomass burning emissions, Environ. Res. Lett., 8, 044042, 10.1088/1748-9326/8/4/044042, 2013.

Srinivas, B., Rastogi, N., Sarin, M. M., Singh, A., and Singh, D.: Mass absorption efficiency of light absorbing organic aerosols from source region of paddy-residue burning emissions in the Indo-Gangetic Plain, Atmos. Environ., 125, 360-370, 10.1016/j.atmosenv.2015.07.017, 2016.

Stedmon, C. A. and Bro, R.: Characterizing dissolved organic matter fluorescence with parallel factor analysis: a tutorial, Limnol. Oceanogr. Meth., 6, 572-579, 10.4319/lom.2008.6.572, 2008.

Tang, X., Zhang, X., Wang, Z., and Ci, Z.: Water-soluble organic carbon (WSOC) and its temperature-resolved carbon fractions in atmospheric aerosols in Beijing, Atmos. Res., 181, 200-210, 10.1016/j.atmosres.2016.06.019, 2016.

Wu, C. and Yu, J. Z.: Determination of primary combustion source organic carbon-to-elemental carbon (OC / EC) ratio using ambient OC and EC measurements: secondary OC-EC correlation minimization method, Atmos. Chem. Phys., 16, 5453-5465, 10.5194/acp-16-5453-2016, 2016.

Xie, X., Chen, Y., Nie, D., Liu, Y., Liu, Y., Lei, R., Zhao, X., Li, H., and Ge, X.: Light-absorbing and fluorescent properties of atmospheric brown carbon: A case study in Nanjing, China, Chemosphere, 251, 126350, 10.1016/j.chemosphere.2020.126350, 2020.

Yu, J., Xiao, K., Xue, W., Shen, Y.-x., Tan, J., Liang, S., Wang, Y., and Huang, X.: Excitation-emission matrix (EEM) fluorescence spectroscopy for characterization of organic matter in membrane bioreactors: Principles, methods and applications, Front. Env. Sci. Eng., 14, 31, 10.1007/s11783-019-1210-8, 2020.

Zhan, Y., Li, J., Tsona, N. T., Chen, B., Yan, C., George, C., and Du, L.: Seasonal variation of water-soluble brown carbon in Qingdao, China: Impacts from marine and terrestrial emissions, Environ. Res., 212, 10.1016/j.envres.2022.113144, 2022.

Zhang, J., Qi, A., Wang, Q., Huang, Q., Yao, S., Li, J., Yu, H., and Yang, L.: Characteristics of water-soluble organic carbon (WSOC) in PM2.5 in inland and coastal cities, China, Atmospheric Pollution Research, 13, 101447, 10.1016/j.apr.2022.101447, 2022.

Zhang, Y., Ma, X., Tang, A., Fang, Y., Misselbrook, T., and Liu, X.: Source Apportionment of Atmospheric Ammonia at 16 Sites in China Using a Bayesian Isotope Mixing Model Based on δ15N–NHx Signatures, Environ. Sci. Technol., 57, 6599-6608, 10.1021/acs.est.2c09796, 2023.

Zhao, S., Qi, J., and Ding, X.: Characteristics, seasonal variations, and dry deposition fluxes of carbonaceous and water-soluble organic components in atmospheric aerosols over China's marginal seas, Mar. Pollut. Bull., 191, 114940, 10.1016/j.marpolbul.2023.114940, 2023.

Zhou, Y., Chen, J., Fan, F., Feng, Y., Wang, S., Fu, Q., and Feng, J.: Deconvolving light absorption properties and influencing factors of carbonaceous aerosol in Shanghai, Sci. Total Environ., 839, 156280, 10.1016/j.scitotenv.2022.156280, 2022.